
Assessment of ^{11}C -PE2I Binding to the Neuronal Dopamine Transporter in Humans with the High-Spatial-Resolution PET Scanner HRRT

Claire Leroy¹, Claude Comtat², Régine Trébossen², André Syrota², Jean-Luc Martinot¹, and Maria-João Ribeiro^{1,2}

¹CEA-INSERM U797 Research Unit Neuroimaging in Psychiatry, Service Hospitalier Frédéric Joliot, IFR49, Orsay, and University of Paris-sud, Paris, France; and ²CEA, DRM, DSV, Service Hospitalier Frédéric Joliot, Orsay, France

The high-resolution research tomograph (HRRT), dedicated to brain imaging, may offer new perspectives for identifying small brain nuclei that remain neglected by the spatial resolution of conventional scanners. However, the use of HRRT for neuroimaging applications still needs to be fully assessed. The present study aimed at evaluating the HRRT for measurement of the dopamine transporter (DAT) binding to validate its quantification and explore the gain induced by the increased spatial resolution in comparison with conventional PET scanners. **Methods:** Fifteen and 11 healthy subjects were examined using the selective DAT radioligand ^{11}C -PE2I with HRRT and HR+ scanners, respectively. Quantification of the DAT binding was assessed by the calculation of binding potential (BP) values using the simplified reference tissue model in anatomic regions of interest (ROIs) defined on the dorsal striatum and in a standardized ROI defined on the midbrain. **Results:** Quantification of ^{11}C -PE2I binding to the DAT measured in the midbrain and striatum with both scanners at the same spatial resolution (smoothed HRRT images) exhibited similar BP values and intersubject variability, thus validating the quantification of DAT binding on the HRRT. For age-paired comparison, BP values of subjects examined with HRRT were significantly higher than those of the subjects examined with HR+. The increase ranged from 29% in the caudate and 35% in the putamen to 92% in the midbrain. The decline in DAT binding with age in the striatum was in good agreement between both scanners and literature, whereas no significant decrease in DAT binding with age was observed in the midbrain with either HRRT or HR+. **Conclusion:** HRRT allows quantitative measurements of neurotransmission processes in small brain nuclei and allows recovering higher values as compared with coarser spatial resolution PET scanners. High-spatial-resolution PET appears promising for a more accurate detection of neurobiologic modifications and also for the exploration of subtle modifications in small and complex brain structures largely affected by the partial-volume effect.

Key Words: brain PET; high spatial resolution; high-resolution research tomography; dopamine transporter

J Nucl Med 2007; 48:538–546

DOI: 10.2967/jnumed.106.037283

An active field in nuclear medicine instrumentation research is the development of high-resolution PET that reaches an isotropic spatial resolution of <3 mm in the reconstructed images. Therefore, high-resolution PET for human cerebral application appears promising for the exploration of subtle neurobiologic modifications as well as for the identification of small brain nuclei that remain limited by the spatial resolution of whole-body scanners.

The high-resolution research tomograph ECAT HRRT (Siemens Medical Solutions) is the only human brain commercial scanner with an isotropic spatial resolution of <3 mm in all 3 directions for a 20-cm-diameter central field of view (FOV) (1). In comparison, the previous generation of scanner, such as the whole-body ECAT EXACT HR+ scanner (Siemens Medical Solutions), has a radial intrinsic resolution of >5.7 mm over a 20-cm-diameter FOV (2). This latter scanner has been used routinely for cerebral imaging for 10 y. The >6 -fold improvement of the HRRT intrinsic volumetric resolution against the HR+ should offer a better accuracy in the measurement of radioactivity concentrations in small volumes by reducing the partial-volume effect. However, to fully benefit from the high-resolution technology of the HRRT, it is necessary to use specific algorithms for image reconstruction based on 3-dimensional (3D) iterative reconstruction methods (3). The use of high-resolution and 3D iterative reconstruction techniques still needs to be assessed for neuroimaging applications.

Here, we investigated the impact of the gain in spatial resolution of HRRT on the dopaminergic transmission determination by measurement of the regional ^{11}C -PE2I binding to the neuronal dopamine transporter (DAT). The DAT is localized on the presynaptic sites of the dopaminergic neurons and ensures the reuptake of the synaptic dopamine into the presynaptic space (4). Thus, DAT appears as a specific marker of the dopaminergic neurons and acts as a key factor in the regulation of the dopaminergic neurotransmission. Modifications of DAT availability have already been shown in vivo and in postmortem studies in neurologic

Received Oct. 16, 2006; revision accepted Dec. 27, 2006.
For correspondence or reprints contact: Claire Leroy, PhD, CEA-INSERM U797, Service Hospitalier Frédéric Joliot, 4 place du Général Leclerc, 91401 Orsay cedex, France.
E-mail: claire.leroy@cea.fr
COPYRIGHT © 2007 by the Society of Nuclear Medicine, Inc.

disease, such as Parkinson's disease, and in psychiatric and addictive disorders, such as depression, schizophrenia, attention-deficit hyperactivity disorder, and alcoholism (5). Most PET studies focused on measurement of the DAT availability in the striatum, which represents a large dopaminergic area with the highest DAT density of the brain. Nonetheless, measurement of DAT binding in other small dopaminergic regions, such as midbrain, from which dopaminergic innervations originate, appears to be of central interest for the pathophysiology of several neurologic and psychiatric disorders. Whereas postmortem studies reported extrastriatal DAT density (6,7), in vivo determination of extrastriatal DAT binding remains limited (8,9). Telang et al. had success in studying DAT binding in the thalamus and limbic and paralimbic brain of living human brain with ^{11}C -cocaine by averaging the distribution-volume PET images of a cohort of 17 control subjects (10). In the present study, we assessed the reliability of the use of the HRRT scanner as a necessary step for the prospect of further clinical studies using high-spatial-resolution PET technology. Whereas the use of whole-body scanners such as HR+ has largely been documented and validated for brain imaging, specific data processing of the HRRT still needs to be assessed. Therefore, we first evaluated the quantification of the regional ^{11}C -PE2I binding to the DAT in the striatum and midbrain using HRRT in healthy subjects. Hence, we compared DAT quantification in HR+ images and HRRT images matched to HR+ spatial resolution. Second, we evaluated the gain of the higher spatial resolution of HRRT on this quantification by comparing values obtained from 2 age-matched groups of healthy subjects scanned on either HR+ or HRRT at scanner resolution. Because 2 biomedical research protocols were engaged at the same time using ^{11}C -PE2I and the same methodology, one with the HR+ and the other with the HRRT, we decided to avoid injecting volunteers twice with the same radioligand for a study of instrumentation validation. Consequently, the imaging data compared in this study between both scanners were obtained from 2 different groups of healthy subjects. This procedure led us to compare whole samples as well as subgroups restrained to age-matched subjects.

MATERIALS AND METHODS

Subjects

Two different groups of healthy volunteers were examined on either HRRT or HR+ scanners. Fifteen volunteers (30.8 ± 8.6 y; range, 19–47 y) were examined using the HRRT scanner and 11 volunteers (46.4 ± 7.3 y; range, 35–57 y) were examined using the HR+ scanner. For an age-paired comparison, 6 of the 15 subjects (39.3 ± 5.9 y) examined with HRRT were compared with 6 age-paired of the 11 subjects (41.2 ± 4.7 y) examined with HR+. None of the subjects had a history of neurologic or psychiatric diseases. All volunteers gave their written informed consent after receiving a detailed explanation of the procedure. The study protocol was approved by local biomedical ethical committees.

Description of Scanners

Two 3D PET scanners were used: an ECAT EXACT HR+ (HR+) and the second-generation ECAT HRRT (HRRT).

The HR+ is a whole-body scanner with a 58.3-cm transaxial and 15.5-cm axial FOV (63 image slices of 2.4-mm thickness). The attenuation coefficients are measured using three ^{68}Ge transmission rod sources.

The HRRT is a dedicated brain imaging system with a 31.2-cm transaxial and 25.5-cm axial FOV (207 image slices of 1.2-mm thickness). The second-generation HRRT is made of $2.1 \times 2.1 \times (10 + 10)$ mm³ dual-layer lutetium oxyorthosilicate (LSO) and lutetium-yttrium oxyorthosilicate (LYSO—i.e., 70% YSO and 30% LSO) crystals. This crystal configuration allows the scanner to measure depth of interaction, preserving a good spatial resolution toward the edge of the transverse FOV. The attenuation coefficients are measured using a ^{137}Cs transmission point source.

Data Acquisition and Processing

MRI Acquisition. For all subjects, T1-weighted 3D images were acquired using a 1.5-T Signa system scanner (General Electric Healthcare). MRI parameters included axial slices of 1.3-mm thickness, a FOV of 24 cm, and an acquisition matrix of $256 \times 256 \times 128$ voxels, with a voxel's size of $0.94^2 \times 1.3$ mm³. Anatomic MRI was performed for accurate MRI/PET coregistration and image analysis.

PET Acquisition. The acquisition protocol was similar for both scanners. The subjects were positioned in the scanner using a 2-dimensional laser alignment. A thermoplastic head mask was molded to each subject's face to restrain head movements. A transmission scan was performed before the intravenous injection of radiotracer to correct for γ -ray attenuation. ^{11}C -PE2I was used as the radioligand of the neuronal DAT, and it was synthesized according to previously described methods (11,12). The dynamic acquisition started at the bolus injection and lasted for 60 min.

On the HR+, the tissue attenuation was measured using a 15-min transmission scan. The mean intravenously injected dose of ^{11}C -PE2I for the whole sample of subjects was 275.2 ± 28.0 MBq, with a mean specific radioactivity of 41.6 ± 13.8 GBq/ μmol . The HR+ images were reconstructed with the standard analytic 3D filtered reprojected algorithm (3DRP (13)) and a Hann low-pass apodization window with a cutoff at the Nyquist frequency. This reconstruction algorithm has been used routinely on the HR+ for brain imaging over the last 10 y and is considered as a well-validated technique. The voxel size was $2.4 \times 2.4 \times 2.4$ mm³.

On the HRRT, the tissue attenuation was measured using a 6-min transmission scan. The attenuation map was segmented into air, soft-tissue, and bone compartments. The mean intravenously injected dose of ^{11}C -PE2I was 302.0 ± 46.5 MBq, with a mean specific radioactivity of 22.4 ± 8.5 GBq/ μmol . The HRRT images were reconstructed with the iterative ordered-subset expectation maximization (OSEM) 3D method, with corrections for random and scattered coincidences, attenuation, and normalization included in the reconstruction (Ordinary Poisson [OP]-OSEM 3D (3)). Sixteen subsets were used, and the reconstruction was run for 6 iterations, ensuring convergence of the average voxel value within the anatomic regions of interest (ROIs) used in the study. The voxel size was $1.2 \times 1.2 \times 1.2$ mm³.

For the reconstruction protocols used in this study, the spatial resolution is close to 2.5 mm for the HRRT images and close to 7.0 mm for the HR+. To compare the HRRT and the HR+ data at matched partial-volume effect, it is necessary to degrade the

spatial resolution of the HRRT images. A point source was acquired on both scanners for radial distances varying between 1 and 10 cm and reconstructed using the reconstruction protocols described above. It was found that the best match in spatial resolution between both scanners was for the HRRT images smoothed with a 5.5-mm full width at half maximum 3D isotropic and stationary Gauss kernel. Two sets of HRRT images were used in the comparative study: one set at the nominal 2.5-mm spatial resolution (native HRRT) and one set smoothed after reconstruction with a 5.5-mm 3D Gauss kernel (smoothed HRRT). This second set has, on average, the same amount of partial-volume effect in the brain as the HR+ images.

Data Analysis

The 3 sets of PET images were analyzed using a compartmental model approach by quantifying the binding potential (BP) within ROIs defined on the dorsal striatum and the dorsal midbrain (substantia nigra and ventral tegmental area). The BP values obtained illustrate the specific binding of ^{11}C -PE2I to the DAT and are expressed as mean \pm SD.

Two different approaches were used for the quantification of BP in dorsal striatum and midbrain:

- Dorsal Striatum and Cerebellum. Anatomic ROIs were defined individually for each subject. ROIs were drawn on the dorsal caudate nucleus, dorsal putamen, and cerebellum on the individual reconstructed MR images (Fig. 1A). After a mutual information coregistration between MRI and PET images, the ROIs were transposed over the PET slice to extract the mean activity concentration values. The mean activity concentration values in the ROIs for the caudate, putamen, and cerebellum were calculated and used to generate regional time-activity curves. These time-activity curves were used to calculate the ^{11}C -PE2I BP to the DAT in each striatal structure using the Simplified Reference Tissue Model (SRTM) of Lammertsma and Hume (14), with the cerebellum as reference tissue. For that calculation, the general modeling tool of the Pmod software was used (Pmod2.65; PMOD Technologies Ltd.). This modeling approximates the tissue of interest as a single tissue compartment and assumes that both the

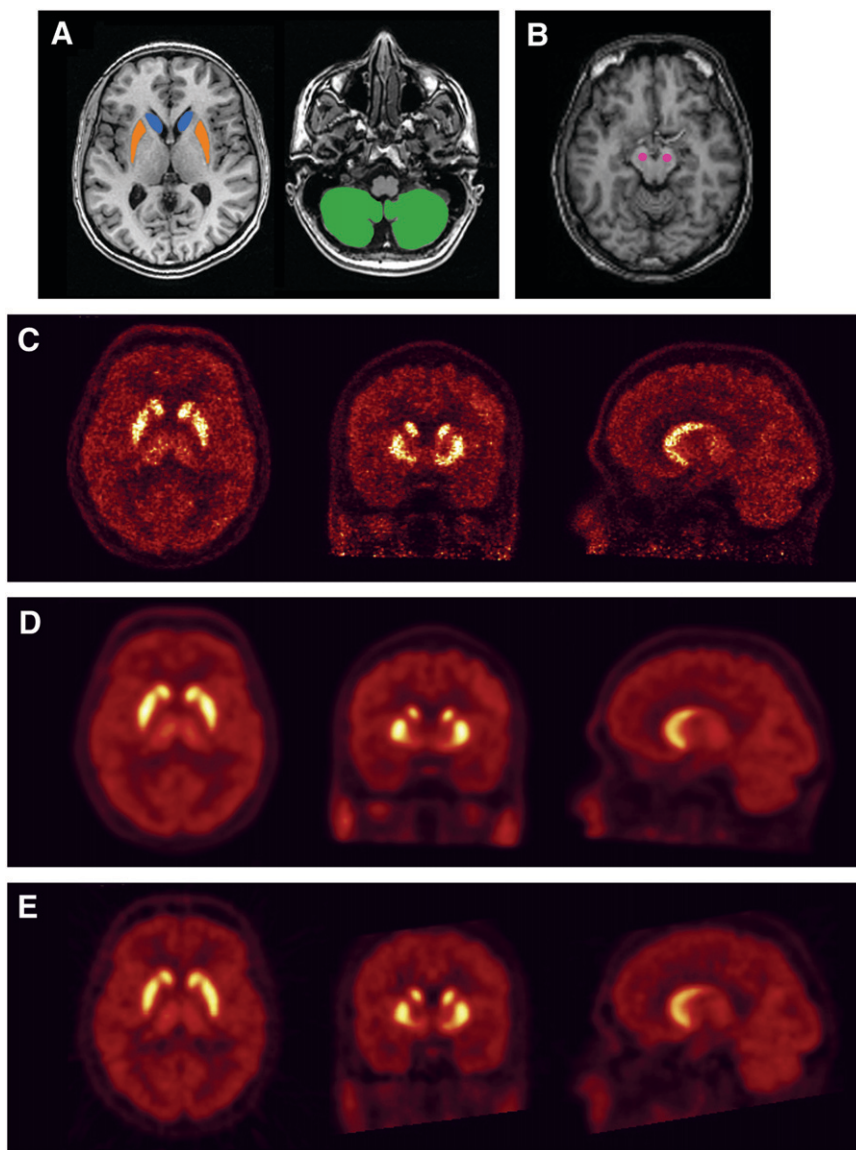


FIGURE 1. Examples of MRI and PET images. (A) MRI axial planes show delineation of anatomic ROIs in caudate (blue color), putamen (orange color), and cerebellum (green color). (B) Normalized MRI axial plane shows geometric ROIs in midbrain (pink color). (C–E) HRRT and HR+ coregistered frame-summed PET images on axial (left), coronal (middle), and sagittal (right) planes: native HRRT (C), smoothed HRRT (D), and HR+ (E).

tissue of interest and the reference region have the same level of nondisplaceable radioligand binding. Previous studies validated the suitability of quantification of specific ^{11}C -PE2I binding using a compartmental approach with reference region (15).

- Dorsal Midbrain. Geometric standardized ROIs were drawn on normalized parametric PET images (Fig. 1B). Dopaminergic regions of the midbrain are small (average ROI sizes are given in Table 1) and barely distinguishable on MR images. Parametric mapping was performed to alleviate the statistical noise related to very small ROIs that renders the measurement of BP using SRTM not robust (see Discussion). The choice of doing normalization was undertaken to reduce the interindividual variability in brain anatomy and to avoid errors by the operator in defining ROI in midbrain individually for each subject. Parametric images were generated with the pixelwise tool of Pmod. This tool generates BP maps with time–activity vector in each individual pixel. The Gunn’s Basis Function Method (BFM), implemented according to Gunn et al., was used (16). This method aims at making the SRTM more robust for pixelwise applications and is closely related to SRTM. Therefore, BFM is also well suited for BP analysis of very small regions such as the midbrain. As for the SRTM, the cerebellum regional time–activity curve was provided for the reference tissue. The BP parametric images were normalized using the Statistical Parametric Mapping software (17), version 2 (SPM2; Wellcome Department of Cognitive Neurology), and Matlab 6.5 for Linux (Math Works). The spatial normalization of parametric images implies scanner-specific ^{11}C -PE2I BP templates constructed according to the MRI-based spatial normalization approach of Meyer et al. (18). The same normalization matrix was used for both datasets of HRRT images. Such a procedure was validated previously and used in several studies (19,20). A spheric ROI was drawn at the level of the dorsal midbrain on a T1 MR image of MNI (Montreal Neurologic Institute database). Before ROI analysis, we checked this processing by overlapping PET parametric images and T1 MR image representing brain anatomy in accordance with the MNI space. Moreover, to assess the reliability of quantification of DAT binding in midbrain from standardized ROI on normalized parametric PET images, we checked the consistency of the procedure for the whole sample of healthy subjects as follows: We correlated the striatal BP values obtained from

anatomic ROIs drawn on native PET images for the dorsal striatum with striatal BP values obtained from a standardized ROI drawn on normalized parametric BP images. Even if the ROIs were not exactly the same between normalized and nonnormalized images, the BP values obtained from both sets of images were in good agreement ($n = 26$; Pearson correlation coefficient = 0.885; $P < 0.0001$).

Statistical Analysis

The statistical analysis of the comparison between the regional BPs for ^{11}C -PE2I of groups scanned on HR+ and HRRT was performed with the nonparametric Mann–Whitney U test. The statistical analysis between the regional BPs for ^{11}C -PE2I from native HRRT images and smoothed HRRT images was performed with Wilcoxon rank tests. The comparison of variances of mean BP values obtained from HR+ and both sets of HRRT images was performed with F tests for variances. According to van Dyck et al., who showed that the linear model provides a reasonable age correction for the study of DAT (21), the age and the radioactive specific activity effects on DAT binding were examined by linear regression analyses. In all analyses, the statistical significance was set at $P < 0.05$.

RESULTS

The group examined with HRRT (30.8 ± 8.6 y) was significantly younger than that studied with HR+ (46.4 ± 7.3 y) ($U = 15.5$; $P < 0.0001$). However, the mean age of subgroups for age-paired comparison did not differ significantly ($U = 15.5$; $P = 0.7$).

Whereas the mean injected dose was not statistically different between groups ($U = 55$; $P = 0.2$ for the entire groups and $U = 17$; $P = 0.9$ for age-paired groups), the mean radioactive specific activity between groups was significantly different, considering the whole samples (42 ± 14 and 22 ± 9 GBq/ μmol for HR+ and HRRT, respectively; $U = 147$; $P = 0.001$) as well as the age-paired populations (45 ± 17 and 25 ± 10 GBq/ μmol for HR+ and HRRT, respectively; $U = 31$; $P = 0.03$). Taking into account this large difference in specific activity, we have checked the influence of radioactive specific activity on the BP values for the 2 whole samples of subjects by linear

TABLE 1
BP Values in Dorsal Striatum and Midbrain for 3 Sets of Images for Age-Paired Subjects

Dopaminergic region	BP value (mean \pm SD)			% increase in BP value: native HRRT/HR+	Average ROI volume (mm ³)
	HR+	Native HRRT	Smoothed HRRT		
Dorsal striatum	6.8 \pm 1.2	8.9 \pm 1.1*†	7.5 \pm 0.7	+32.3	12,590 \pm 1,465
Dorsal caudate	6.3 \pm 0.9	8.1 \pm 1.4*†	6.9 \pm 1.0	+29.2	6,816 \pm 971
Dorsal putamen	7.2 \pm 1.1	9.7 \pm 1.2*†	8.2 \pm 0.8	+35.1	5,774 \pm 854
Midbrain	1.1 \pm 0.3	2.2 \pm 0.1*	1.0 \pm 0.3	+92.4	830

* $P < 0.005$ statistically different from HR+ images (Mann–Whitney U test).

† $P < 0.05$ statistically different from smoothed HRRT images (Wilcoxon rank test).

Volume of anatomic ROIs in cerebellum and striatum (mean \pm SD) as well as volume of standardized ROIs in midbrain are expressed in mm³.

regression analyses, including age as the controlling variable. No correlation was found between specific activity and BP values either for HRRT data or for HR+ data for the striatum ($df = 12$; $r = 0.22$; $P = 0.5$ and $df = 8$; $r = 0.145$; $P = 0.7$, respectively) and the midbrain ($df = 12$; $r = 0.273$; $P = 0.4$ and $df = 8$; $r = -0.527$; $P = 0.1$, respectively).

The visual inspection of the frame-summed PET images (Figs. 1C–1E) showed that the native HRRT images had a better delineation of cortical gyri as well as subcortical nuclei in comparison with smoothed HRRT and HR+ images, which underwent a coarser and relatively similar structural definition of brain structures. The native HRRT images showed the well-known checkerboard effect of noise due to the OSEM reconstruction algorithm.

Dorsal Striatum

Comparison of BP Values Resulting from HRRT and HR+ Acquisitions. For the entire cohort of subjects, the mean BP values were 8.8 ± 1.2 and 5.6 ± 1.1 in the caudate and 10.5 ± 1.4 and 6.5 ± 1.2 in the putamen for native HRRT and HR+ images, respectively. The interindividual variability of BP was not statistically different between the 2 scanner acquisitions in the caudate ($F = 1.219$; $df = 14$; $P = 0.7$) and the putamen ($F = 1.337$; $df = 14$; $P = 0.6$). BP values obtained using HRRT were significantly increased by 58.5% ($U = 4$; $P < 0.0001$) for the caudate and 61.7% ($U = 1$; $P < 0.0001$) for the putamen in comparison with those obtained using HR+. The mean striatal BP value obtained using HRRT was significantly higher ($U = 2$; $P < 0.0001$) by 60.2% than those obtained using HR+ (9.7 ± 1.1 and 6.0 ± 1.1 for native HRRT and HR+, respectively).

We observed a significant decrease in the DAT binding with increasing age for data from native HRRT ($n = 15$; $r = 0.662$; $P = 0.007$) and smoothed HRRT ($n = 15$; $r = 0.636$; $P = 0.01$) images. With regard to HR+ data, we observed a similar tendency of the age effect on DAT binding that is clearly seen in Figure 2 but was not statistically significant ($n = 11$; $r = 0.544$; $P = 0.08$), primarily due to the smaller subject sample as well as the smaller age range. This age effect appeared similar for caudate and putamen. Thus, the decrease in DAT binding with increasing age in global striatum was 8.1%, 7.2%, and 11.9% per decade for native HRRT, smoothed HRRT, and HR+ images, respectively. The difference between BP values in striatum of the entire sample of subjects obtained using native HRRT and HR+ reflected confounding effects of age difference in both groups as well as the different spatial resolution of both scanners. This confounding effect was confirmed by the BP values obtained from smoothed HRRT images that remained significantly higher than those from HR+ images by 34.2% for the caudate (7.4 ± 1.0 ; $U = 18$; $P = 0.001$) and 32.8% for the putamen (8.6 ± 0.9 ; $U = 13$; $P < 0.001$).

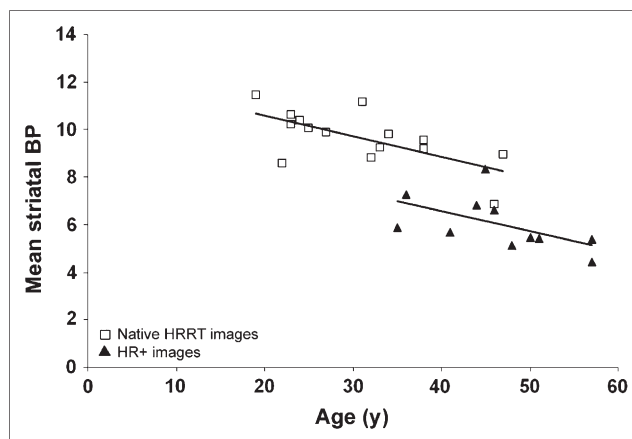


FIGURE 2. Distribution plots show relationship between mean striatal BP value and age of subject. BP values resulted from anatomic ROIs in 15 subjects examined with HRRT and 11 subjects examined with HR+.

Comparison in Age-Paired Groups of BP Values Resulting from HRRT and HR+ Acquisitions. In age-paired group comparison, the effect of age difference was removed, leading essentially to the assessment of the effect of the spatial resolution of both scanners on the measurement of BP values only. The mean regional time–activity curves in Figure 3 show the mean tissue radioactivity over time in the striatum and cerebellum for the 3 sets of images. The profiles of ^{11}C -PE2I accumulation in cerebellum were the same for the 3 sets of images. No significant difference in time–activity curves in striatum was observed between HR+ and smoothed HRRT images. Nevertheless, we observed a higher activity concentration in striatum in native HRRT images in comparison with that of HR+ and smoothed HRRT images.

The BP values obtained from the 3 sets of images are summarized in Table 1. The mean BP values resulting from native HRRT were significantly higher than those obtained using HR+ and smoothed HRRT images for the caudate as

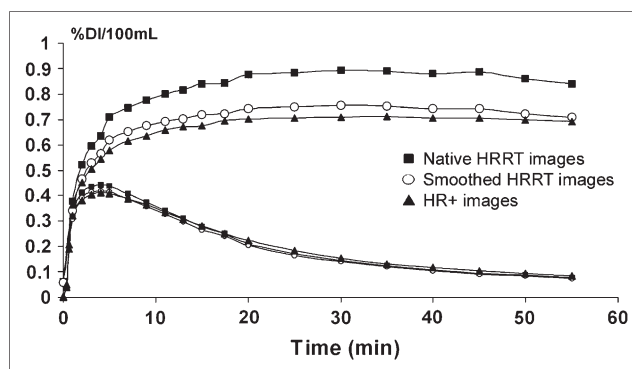


FIGURE 3. Average time–activity curves, normalized to injected dose (%DI/100 mL) of ^{11}C -PE2I, in dorsal striatum and cerebellum, for age-paired subjects examined with HR+ and HRRT scanners.

well as for the putamen. The difference between native HRRT images and HR+ images represented a 29.2% and 35.1% increase in BP values for the caudate ($U = 4$; $P = 0.025$) and the putamen ($U = 1$; $P = 0.007$), respectively. However, BP values measured on smoothed HRRT images did not differ from those measured on HR+ images for the caudate ($U = 12$; $P = 0.3$) and the putamen ($U = 8$; $P = 0.1$). The nearly 7% higher BP values of smoothed HRRT images than those of HR+ images were below the inter-individual variability of BP values observed in this study (ranging from 11.8% to 20.2%).

Midbrain

Comparison of BP Values Resulting from HRRT and HR+ Acquisitions. For the entire cohort of subjects, the mean BP values were 2.3 ± 0.3 and 1.0 ± 0.3 for native HRRT and HR+ images, respectively. BP values obtained using native HRRT appeared highly significantly increased by 129.8% in comparison with BP values obtained using HR+ ($U = 0$; $P < 0.0001$). The interindividual variability of BP values did not differ statistically between the 2 scanner acquisitions ($F = 0.899$; $df = 14$; $P = 0.9$): 28% for HR+ images and 11.5% for native HRRT images. For both scanner acquisitions, we observed a tendency of DAT binding to decrease with age that did not reach a significant level (Fig. 4). This tendency was clearly seen with HR+ and smoothed HRRT images but was quasi-nonexistent with native HRRT images. The mean BP value obtained from smoothed HRRT images was 1.3 ± 0.4 . This value was significantly lower in comparison with that obtained from native HRRT images ($z = -3.408$; $P = 0.0007$), but did not differ significantly from that obtained with HR+ images ($U = 46$; $P = 0.06$).

Comparison in Age-Paired Groups of BP Values Resulting from HRRT and HR+ Acquisitions. Results from age-matched comparison were similar to that from the comparison performed on the whole sample (Table 1). BP values obtained from native HRRT images were highly significantly increased

by 92.4% and 122.6% in comparison with BP values obtained using HR+ ($U = 0$; $P = 0.004$) and smoothed HRRT ($z = -2.201$; $P = 0.03$) images. Results from smoothed HRRT and HR+ images remained not significantly different ($U = 15$; $P = 0.6$).

DISCUSSION

The present study first validated the quantification of DAT binding with HRRT and ^{11}C -PE2I. For that purpose, we have shown that despite the different modalities of image reconstruction between HRRT and HR+ scanners, BP values were comparable at same spatial resolution. On the basis of this preliminary result, we assessed the effective gain of higher spatial resolution of native HRRT images on BP measurement, and we have shown that, in an age-matched population, the HRRT allows recovering higher values of the BP of ^{11}C -PE2I to the DAT of approximately 30% in the striatum and 90% in the midbrain as compared with values measured using HR+.

One study was reported using HRRT for the measurement of biologic parameters in human brain with ^{18}F -FDG (22). This study showed that HRRT permits both the quantification of the regional cerebral metabolic rates for glucose in smaller volumes and also a better accuracy in large brain areas in comparison with that reported previously with conventional scanners. Though promising to extend the use of HRRT with various radiotracers, application studies on a sample of healthy subjects are needed to allow further applications and developments. The present study reports, to our knowledge, the first validation of the examination of a neurotransmission system using the HRRT tomograph. Because of the small size of the structures involved, we chose to explore the dopaminergic system via the measurement of DAT with ^{11}C -PE2I for the validation and the assessment of the gain of high resolution on exploration of the neurotransmission system.

Several aspects facilitated the comparison between scanners of the DAT binding with ^{11}C -PE2I. First, there is a large documentation of measurements of DAT binding in vitro and with conventional PET and SPECT scanners (23). Second, the SRTM has been shown to be reliable for the measurement of DAT binding with ^{11}C -PE2I (15), and this radiotracer was recently presented as well adapted for the examination of the dopaminergic regions of the midbrain, such as substantia nigra and ventral tegmental area (8,11,15).

The comparison of time-activity curves and BP values obtained with the HR+ with those obtained with HRRT images matched at HR+ spatial resolution allowed us to estimate the suitability of our quantification of DAT binding with ^{11}C -PE2I using HR+ and HRRT. The mean time-activity curves obtained from HR+ and smoothed HRRT images showed quite similar values in striatum and cerebellum. There is no evidence of a biased HRRT quantification in the cerebellum that can be due, for example, to a biased scatter correction. As some studies choose the

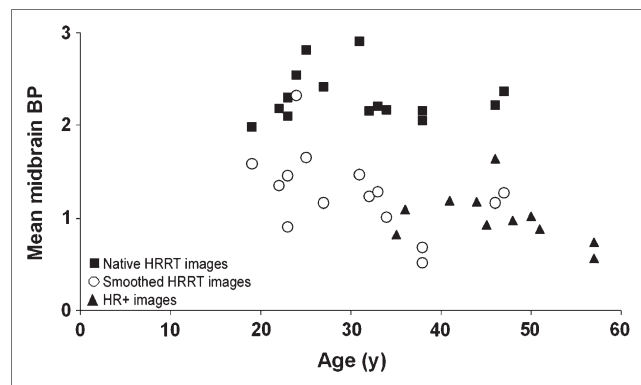


FIGURE 4. Distribution plots show relationship between mean midbrain BP values and age of subjects. BP values resulted from “standard-MNI” ROIs in 15 subjects examined with HRRT at spatial resolution of HRRT (native HRRT images) and HR+ (smoothed HRRT images) and 11 subjects examined with HR+.

occipital region as reference tissue, we checked that the time–activity curves in the occipital region were similar to that obtained in the cerebellum (data not shown). The mean BP values of caudate, putamen, and midbrain from HR+ and smoothed HRRT images were comparable and consistent with previous published data using PET scanners at similar spatial resolution (8,15). Although the midbrain ROI delineation method in the study of Jucaite et al. differed from ours, similar magnitudes of BP values and intersubject variability were observed (8). Thus, this preliminary assessment shows that it is possible to reproduce results obtained with HR+ using HRRT images at matched spatial resolution.

Both groups of subjects were not composed of the same volunteers. Thus, each subject received one dose of radiotracer instead of 2. This is a limitation of the study that combines the effect of intersubject variability with the effect of difference in scanner performance. However, for age-paired comparison, the differences in BP values between HR+ and smoothed HRRT images did not exceed 7% for both striatum (6.8 ± 1.2 vs. 7.5 ± 0.7) and midbrain (1.1 ± 0.3 vs. 1.0 ± 0.3)—that is, remained below the interindividual variability of the BP values observed. Moreover, whereas no test–retest data are available with the radioligand ^{11}C -PE2I, most of the test–retest studies reported in neurotransmission imaging showed a variability within a subject ranging from 0% to 12% (24,25).

For both scanners and both spatial resolutions, evaluation of DAT binding in a wide age range of subjects confirmed the well-known decline in DAT binding with age in the striatum. The slope of the age effect on DAT binding was consistent between both scanners and with literature, showing a decrease in the DAT density of approximately 6.6%–9% per decade in striatum in postmortem (26,27) and in vivo (21) studies. Conversely, we did not observe any evidence of an age effect on DAT binding in midbrain either with HRRT or with HR+, consistent with another PET study (8) but at variance with postmortem studies showing age-related DAT messenger RNA and protein expression (28,29). The scatter correction for the HRRT, though using the same algorithm as for the HR+ (30), is known not to be optimal yet because, in part, of the phoswich configuration of the detectors. To evaluate the impact of potentially biased scatter correction on the estimation of the DAT binding, one HRRT subject acquisition was reprocessed twice, with a 5% increased and a 5% decreased scatter estimation (the study of van Velden et al. reported a remnant scatter fraction after correction of 5% for the HRRT, using the NEMA NU 2-2001 standard for brain scanners (31)). These changes result in a variability of the BP value of 7% for the striatum and 2% for the midbrain. A potentially inaccurate scatter correction does not explain the lack of an age effect for the HRRT data. Absence of any evidence of a decrease in DAT binding with age in midbrain PET studies might be related to the limitation of the subject sample sizes. In addition, the small size of the midbrain structure, when

compared with the striatum, results in a higher level of statistical variability, in particular for the native HRRT images, that can impair the detection of an age effect.

The main objective was to evaluate the gain induced by a higher spatial resolution on the measurement of DAT binding. HRRT improves consistently the quantification of DAT binding due to a reduced partial-volume effect in comparison with HR+. This improvement appears more important when the brain structure is small and largely affected by the partial-volume effect. In this context, the examination of the small dopaminergic regions of the midbrain (substantia nigra and ventral tegmental area), which constitute key structures of the dopaminergic pathways, were of specific interest to emphasize the benefit of the high spatial resolution. The 2-fold higher DAT binding observed in midbrain using native HRRT images shows that the impact of the high resolution is particularly efficient for the brain regions largely affected by the partial-volume effect on clinical PET scanners (32). In addition, the variation between the native HRRT and the smoothed HRRT images of the midbrain-to-cerebellum regional activity ratio is similar to the variation obtained with phantom measurements, using a contrast sphere of size similar to the midbrain. Thus, the favorable signal-to-background ratio for ^{11}C -PE2I binding in midbrain with HRRT allows the exploration of DAT binding in this brain region that remained limited up to this time (8,11,15). Moreover, this increase in BP values in the midbrain with HRRT is associated with a reduced relative interindividual variability of measures as compared with those obtained with HR+ (11.5% and 28.0% for native HRRT and HR+ images, respectively).

In the striatum, which is a larger brain area than the midbrain, the high resolution improved the quantification of DAT binding in comparison with clinical PET scanners by about 30%. The comparison of time–activity curves obtained from HR+ and native HRRT images showed that the higher value of BP in the striatum is not related to a lower radioactivity concentration measured in the cerebellum on the HRRT images but to a higher radioactivity in the striatum. This behavior was also reported by Sossi et al. for a nonhuman primate study acquired on both an HRRT and an ECAT 953B scanner (33). Higher BP values measured in the striatum with HRRT were most probably due to a reduced partial-volume effect in the quantification of ^{11}C -PE2I binding to the DAT. This observation was corroborated by the similar magnitude of BP values between HR+ and HRRT at same spatial resolution.

To preserve high intrinsic spatial resolution and to account for the scanner's specific geometry, high-resolution imaging using the HRRT requires specific image reconstruction techniques. This reconstruction procedure, based on the OSEM 3D iterative reconstruction algorithm, is not commonly used for brain imaging with clinical scanners, such as the HR+. The quantitative accuracy of iterative reconstructions such as OSEM can be compromised for frames with a very low number of events. On the basis of

brain phantom studies on the HRRT, de Jong et al. reported errors in ROI average values due to the limited statistics that are 10% superior for noise equivalent count rate (NEC) values below 5×10^5 counts (34). Likewise, the study of van Velden et al. reported under- and overestimation of 20% and 50% in the case of short acquisition frames (10–30 s) (31). To limit these low-count-related effects, the shortest frame duration on the HRRT was 60 s. The NEC value was always superior to 1×10^6 counts, except for the first frame (around 5×10^5 counts). The comparison between the smoothed HRRT and the HR+ of the averaged striatum time–activity curve did not reveal any systematic bias for HRRT data. At the level of the voxel, because of its small size (8 times smaller than that for the HR+) and the absence of any regularization such as postreconstruction smoothing, the statistical noise for the native HRRT images is much higher than that for HR+ images (a Hann apodization window is applied during the 3DRP reconstruction). For a relatively large structure such as the putamen or the caudate, the resulting time–activity curve is not very noisy, allowing for a relatively robust regional time–activity curve-based DAT-binding analysis with SRTM. For very small structures such as the midbrain ($<1 \text{ cm}^3$), the statistical noise of the corresponding regional time–activity curve for the native HRRT images was so high that it was not possible to get reliable DAT-binding values based on the midbrain time–activity curve. For this very small structure, the Gunn’s BFM produced an average DAT-binding value for the midbrain with a much lower variability across subjects. Current developments of more advanced OP-OSEM reconstruction algorithms, including a more realistic description of the HRRT system’s response, result in better image quality (better contrast and reduced noise)—in particular, for small structures (35). These image reconstruction developments would be more adapted to estimation of the parameters in very small ROIs ($\leq 1 \text{ cm}^3$) with the SRTM of Lammertsma and Hume (14).

The increased accuracy of measurement with HRRT should allow assessing changes in DAT binding that relate to subtle modifications or small brain nuclei remaining, up to this time, not visible on usual clinical PET scanners. This improved detectability should be useful for the study of addictive or psychiatric disorders such as schizophrenia, where DAT modifications reported are most often of small amplitude and sometimes divergent between imaging studies (36,37). In Parkinson’s disease, degeneration of the nigrostriatal dopaminergic neurons precedes the development of clinical symptoms and results in a loss of DAT (38,39). A more accurate estimation of DAT binding would be useful for the individual diagnosis, follow-up, and estimation of the therapeutic effects of putative neuroprotective agents (40).

CONCLUSION

This study shows the reliability of the HRRT for exploration of the dopamine neurotransmission system. The

enhanced spatial resolution of the HRRT decreases the partial-volume effect in the quantification of DAT binding. This improvement allows a more accurate quantification that permits the examination of minor physiologic events and gives the opportunity to explore small brain nuclei involved in various neurologic and psychiatric disorders. These results are promising for further explorations of biologic parameters in clinical studies with the HRRT.

ACKNOWLEDGMENTS

This study was supported by a grant (SCHIZODAT, APV05143LSA) of the National Agency for Research (ANR) and by the National Institute of Health and Medical Research (INSERM). Support was also provided by a post-doctoral grant from the French Foundation for Medical Research (FRM). The authors thank the nursing and PET technician staffs of the Service Hospitalier Frédéric Joliot for their assistance and the volunteers who participated in this study. We are grateful to Dr. Frédéric Dollé and the radiochemistry staff for the synthesis of the ^{11}C -PE2I. The authors thank anonymous referees for helpful and constructive comments and Drs. Michel Bottlaender and Christian Trichard for thoughtful comments and critical reading of the manuscript.

REFERENCES

1. Sossi V, de Jong HWAM, Barker WC, et al. The second generation HRRT: a multi-centre scanner performance investigation. *Nuclear Science Symposium Conference Record, 2005 IEEE*. 23-29. 2005;4:2195–2199.
2. Herzog H, Tellmann L, Hocke C, et al. NEMA NU2-2001 guided performance evaluation of four Siemens ECAT PET scanners. *IEEE Trans Nucl Sci*. 2004;51:2662–2669.
3. Michel C, Schmand M, Liu X, et al. Reconstruction strategies for the HRRT. *Nuclear Science Symposium Conference Record, 2000 IEEE*. 2000;2:15/207–15/212.
4. Ciliax BJ, Heilman C, Demchyshyn LL, et al. The dopamine transporter: immunochemical characterization and localization in brain. *J Neurosci*. 1995;15:1714–1723.
5. Bannon MJ. The dopamine transporter: role in neurotoxicity and human disease. *Toxicol Appl Pharmacol*. 2005;204:355–360.
6. Hall H, Hallidin C, Guilloteau D, et al. Visualization of the dopamine transporter in the human brain postmortem with the new selective ligand [^{125}I]PE2I. *Neuroimage*. 1999;9:108–116.
7. Little KY, Carroll FI, Cassin BJ. Characterization and localization of [^{125}I]RTI-121 binding sites in human striatum and medial temporal lobe. *J Pharmacol Exp Ther*. 1995;274:1473–1483.
8. Jucaite A, Fernell E, Hallidin C, Forsberg H, Farde L. Reduced midbrain dopamine transporter binding in male adolescents with attention-deficit/hyperactivity disorder: association between striatal dopamine markers and motor hyperactivity. *Biol Psychiatry*. 2005;57:229–238.
9. Sekine Y, Minabe Y, Ouchi Y, et al. Association of dopamine transporter loss in the orbitofrontal and dorsolateral prefrontal cortices with methamphetamine-related psychiatric symptoms. *Am J Psychiatry*. 2003;160:1699–1701.
10. Telang FW, Volkow ND, Levy A, et al. Distribution of tracer levels of cocaine in the human brain as assessed with averaged [^{11}C]cocaine images. *Synapse*. 1999;31:290–296.
11. Hallidin C, Erixon-Lindroth N, Pauli S, et al. [^{11}C]PE2I: a highly selective radioligand for PET examination of the dopamine transporter in monkey and human brain. *Eur J Nucl Med Mol Imaging*. 2003;30:1220–1230.
12. Guilloteau D, Emond P, Baulieu JL, et al. Exploration of the dopamine transporter: in vitro and in vivo characterization of a high-affinity and high-specificity iodinated tropane derivative (E)-N-(3-iodoprop-2-enyl)-2beta-carbomethoxy-3beta-(4'-methylphenyl)nortropane (PE2I). *Nucl Med Biol*. 1998;25:331–337.
13. Kinahan PE, Rogers JG. Analytic three-dimensional image reconstruction using all detected events. *IEEE Trans Nucl Sci*. 1990;36:964–968.

14. Lammertsma AA, Hume SP. Simplified reference tissue model for PET receptor studies. *Neuroimage*. 1996;4:153–158.
15. Jucaite A, Odano I, Olsson H, Pauli S, Halldin C, Farde L. Quantitative analyses of regional [¹¹C]PE2I binding to the dopamine transporter in the human brain: a PET study. *Eur J Nucl Med Mol Imaging*. 2006;33:657–668.
16. Gunn RN, Lammertsma AA, Hume SP, Cunningham VJ. Parametric imaging of ligand-receptor binding in PET using a simplified reference region model. *Neuroimage*. 1997;6:279–287.
17. Friston KJ, Holmes AP, Worsley KJ, Poline JB, Frith CD, Frackowiak RSJ. Statistical parametric maps in functional imaging: a general linear approach. *Hum Brain Mapp*. 1995;2:189–210.
18. Meyer JH, Gunn RN, Myers R, Grasby PM. Assessment of spatial normalization of PET ligand images using ligand-specific templates. *Neuroimage*. 1999;9:545–553.
19. Nagano AS, Ito K, Kato T, et al. Extrastriatal mean regional uptake of fluorine-18-FDOPA in the normal aged brain: an approach using MRI-aided spatial normalization. *Neuroimage*. 2000;11:760–766.
20. Whone AL, Bailey DL, Remy P, Pavese N, Brooks DJ. A technique for standardized central analysis of 6-¹⁸F-fluoro-L-DOPA PET data from a multicenter study. *J Nucl Med*. 2004;45:1135–1145.
21. van Dyck CH, Seibyl JP, Malison RT, et al. Age-related decline in dopamine transporters: analysis of striatal subregions, nonlinear effects, and hemispheric asymmetries. *Am J Geriatr Psychiatry*. 2002;10:36–43.
22. Heiss WD, Habedank B, Klein JC, et al. Metabolic rates in small brain nuclei determined by high-resolution PET. *J Nucl Med*. 2004;45:1811–1815.
23. Bergstrom KA, Tupala E, Tiihonen J. Dopamine transporter in vitro binding and in vivo imaging in the brain. *Pharmacol Toxicol*. 2001;88:287–293.
24. Lundberg J, Halldin C, Farde L. Measurement of serotonin transporter binding with PET and [¹¹C]MADAM: a test-retest reproducibility study. *Synapse*. 2006;60:256–263.
25. Volkow ND, Ding YS, Fowler JS, et al. A new PET ligand for the dopamine transporter: studies in the human brain. *J Nucl Med*. 1995;36:2162–2168.
26. Zelnik N, Angel I, Paul SM, Kleinman JE. Decreased density of human striatal dopamine uptake sites with age. *Eur J Pharmacol*. 1986;126:175–176.
27. Allard P, Marcusson JO. Age-correlated loss of dopamine uptake sites labeled with [³H]GBR-12935 in human putamen. *Neurobiol Aging*. 1989;10:661–664.
28. Bannon MJ, Whitty CJ. Age-related and regional differences in dopamine transporter mRNA expression in human midbrain. *Neurology*. 1997;48:969–977.
29. Ma SY, Ciliax BJ, Stebbins G, et al. Dopamine transporter-immunoreactive neurons decrease with age in the human substantia nigra. *J Comp Neurol*. 1999;409:25–37.
30. Watson CC. New, faster, image-based scatter correction for 3D PET. *IEEE Trans Nucl Sci*. 2000;47:1587–1594.
31. van Velden FHP, Kloet RW, de Jong HWAM, Lammertsma AA, Boellaard R. Quantitative experimental comparison of HRRT versus HR+ PET brain studies. *IEEE Medical Imaging Conference: Conference Record 2006*. 2006: M14-150.
32. Mazziotta JC, Phelps ME, Plummer D, Kuhl DE. Quantitation in positron emission computed tomography. 5. physical-anatomical effects. *J Comput Assist Tomogr*. 1981;5:734–743.
33. Sossi V, Camborde ML, Blinder S, et al. Dynamic imaging on the high resolution research tomograph (HRRT): non-human primate studies. *2005 IEEE Medical Imaging Conference: Conference Record*. 2005:1981–1985.
34. de Jong HWAM, Boellaard R, Michel C, Lammertsma AA. Quantification of dynamic brain studies with the high resolution research tomograph. *2004 IEEE Medical Imaging Conference: Conference Record*. 2004:3730–3732.
35. Sureau F, Comtat C, Reader AJ, et al. Improved clinical parametric imaging using list-mode reconstruction via resolution modeling. *IEEE Medical Imaging Conference: Conference Record 2006*. 2006:M15-6.
36. Spencer TJ, Biederman J, Madras BK, et al. In vivo neuroreceptor imaging in attention-deficit/hyperactivity disorder: a focus on the dopamine transporter. *Biol Psychiatry*. 2005;57:1293–1300.
37. Laakso A, Bergman J, Haaparanta M, et al. Decreased striatal dopamine transporter binding in vivo in chronic schizophrenia. *Schizophr Res*. 2001;52: 115–120.
38. Ribeiro MJ, Vidailhet M, Loc'h C, et al. Dopaminergic function and dopamine transporter binding assessed with positron emission tomography in Parkinson disease. *Arch Neurol*. 2002;59:580–586.
39. Poyot T, Conde F, Gregoire MC, et al. Anatomic and biochemical correlates of the dopamine transporter ligand ¹¹C-PE2I in normal and parkinsonian primates: comparison with 6-[¹⁸F]fluoro-L-dopa. *J Cereb Blood Flow Metab*. 2001;21: 782–792.
40. Stoof JC, Winogrodzka A, van Muiswinkel FL, et al. Leads for the development of neuroprotective treatment in Parkinson's disease and brain imaging methods for estimating treatment efficacy. *Eur J Pharmacol*. 1999;375:75–86.